Quantification of Rare Earth Elements using Laser-Induced Breakdown Spectroscopy

[1]Madhavi Martin, [2]Rodger C. Martin, [1]Steve Allman, [3]Deanne Brice, [1]Ann Wymore, and [4]Nicolas Andre.

[1] Biological Sciences Division,

[2] Fusion and Materials for Nuclear Systems Division, and

[3] Environmental Sciences Division, Oak Ridge National Laboratory, Oak Ridge, TN 37831

[4] The University of Tennessee, Center for Renewable Carbon, Knoxville, TN 37996

Abstract

A study of the optical emission as a function of concentration of laser-ablated yttrium (Y) and of six rare earth elements, europium (Eu), gadolinium (Gd), lanthanum (La), praseodymium (Pr), neodymium (Nd), and samarium (Sm), has been evaluated using the laser-induced breakdown spectroscopy (LIBS) technique. Statistical methodology using multivariate analysis has been used to obtain the sampling errors, coefficient of regression, calibration and cross-validation of measurements as they relate to the LIBS analysis in graphite-matrix pellets that were doped with elements at several concentrations. Each element (in oxide form) was mixed in the graphite matrix in percentages ranging from 1% to 50% by weight and the LIBS spectra obtained for each composition as well as for pure oxide samples. Finally a single pellet was mixed with all the elements in equal oxide masses to determine if we can identify the elemental peaks in a mixed pellet. This dataset is relevant for future application to studies of fission product content and distribution in irradiated nuclear fuels. These results demonstrate that LIBS

technique is inherently well suited for the future challenge of in situ analysis of nuclear materials. These studies also show that LIBS spectral analysis using statistical methodology can provide quantitative results, and suggest an approach in future to the far more challenging multielemental analysis of ~20 primary elements in high-burnup nuclear reactor fuel.

1. Introduction

In nuclear fuel fission reactions, each uranium or plutonium atom will split into two lighter elements. Rare earth elements are a major component of these fission products. Since fission product content in nuclear fuels is proportional to the fraction of "burned" fuel, it can be used to estimate actinide masses (U, Pu, etc.) for nonproliferation "safeguards" monitoring. The reprocessing of irradiated fuel must remove most fission products prior to reuse as fuel. Therefore, it is important to monitor the presence of mixed actinide, rare earths, and other fission product elements throughout the separation process. Challenges in monitoring fission product content using conventional analytical techniques can be significant, such as in electrochemical recycling processes [1]. The emission spectra of rare earths are very complex and spectral interferences must be known, so a detailed and comprehensive study of the predominant rare earths using LIBS has been undertaken in this research and reported here. There are a number of detailed research articles that have shown the LIBS measurements on actinides, their surrogates, [2-7, 27] and rare earth elements [8-26]. This study is the most comprehensive LIBS analysis of rare earth elements individually and in a mixture.

Prior research shows that the technique of LIBS has been used in the elemental analysis of the rare earth elements [8-27]. Among those, europium has been studied the most. Eu^{+} has

been detected in colloidal solutions and the technique has been used in the determination of solubility data and of concentrations of europium in glass matrices [8-13]. Another study has determined trace levels of samarium, europium, and gadolinium in aqueous samples by LIBS [9]. Stainless steel coated gadolinium, and gadolinium in its solid oxide form and in molten glass matrices have been studied [15, 16]. LIBS studies of other rare earths such as lanthanum [14, 17], neodymium [18-22], praseodymium, samarium [27, 23], and yttrium [24-27] have been also been performed.

The rare earths studied here using the LIBS technique are europium (Eu), gadolinium (Gd), lanthanum (La), neodymium (Nd), praseodymium (Pr), samarium (Sm), and the transition metal yttrium (Y). The rationale for selecting these particular elements for the LIBS studies in this article is given by a typical example: in irradiated nuclear reactor fuel, after decay of 150 days, ~18% of the fissions result in Nd atoms, 13% in Ce atoms (previously studied using LIBS [28]), 6% in La and in Pr, 4% in Y and in Sm, 0.6% in Eu, and 0.3% in Gd [29]. There are numerous difficulties associated with undertaking the simultaneous analysis of actinides, rare earths, and other fission products, and extremely dense and complex spectral features result from the as-produced mixture. These difficulties are (i) experimental, (ii) operational, and (iii) safety related. The technique of choice for measuring the actinide and rare earth content in irradiated fuel is ICP-MS or ICP-OES/AES [30-41], but the challenge of analyzing concentrated solutions from fuel dissolution with very high radiological dose must first be addressed. This creates analytical uncertainties from large dilutions, up to a million-fold, which can be costly and time consuming and increase worker hazards in sample handling. Furthermore, complex spectral features can create problems in identification, fingerprinting, and in the quantification of these elements. Operational difficulties often involve burdensome paperwork, approvals, and controls

that are required when handling even <1 g of fissile material such as enriched uranium or plutonium. Setting up glove boxes for radioanalytical work has significant operational costs, and hot cell costs are even higher. Pre-operational safety analysis of new equipment and operations and of radioactive content and its potential for release is far more rigorous than typical laser and chemical safety requirements. In addition to the experimental and operational difficulties, each nuclear facility in the U. S. has "safety basis documents" that set nuclear safety boundaries for experimental activities. Any new hazard introduced into a nuclear facility must be analyzed and documented. This work must be approved prior to beginning new experiments and can take months if not routine. For these reasons, LIBS has certain advantages as a micro-analytical technique in potentially mitigating some of these controls compared to conventional analytical techniques.

As with all analytical techniques, LIBS has inherent limitations that hinder quantification. Due to the matrix effects, true quantitative analyses and calibrations can be a problem. One drawback for the LIBS technique is that different matrices for different samples require matrix-specific calibration standards. Windom and Hahn have overcome the matrix effects for the LIBS technique in their article [42] and also discussions of the challenges for the quantitative analysis for the LIBS technique have been shown in the review articles by Hahn and Omenetto and other authors [43-45]. Certain issues such as sampling geometry on elemental emissions and other sampling parameters have been clearly addressed [46, 47].

For the previously mentioned example of irradiated nuclear reactor fuel after decay of 150 days, the estimates of fission product content [29] indicate that ~23% of the fission product mass is represented by the seven elements measured in this work, which also provides a spectral database of these elements for further LIBS studies. A previous LIBS study of Cs, Sr, and Ce in

the same matrix as here [28] covers another ~18% of this fission product mass and associated

LIBS spectra. Separate LIBS studies of Mo, Zr (in U-Zr alloy form), and Pd contribute spectral

data for another ~24% of the fission product mass. Spectral data from these separate studies can

now be used to plan the LIBS measurement of and interpretation of results for nearly two-thirds

of the fission product content (depending on the time of decay prior to measurement) in

irradiated fuel samples. Synthesis of these spectral libraries with the spectral tabulations from

recent mixed actinide studies [6] of U, Np, Pu, and Am now provides a starting point for analysis

of complex nuclear fuel mixtures, including selection of optimal low-interference identifying

peaks for each element.

In 2003 a feasibility experiment demonstrated LIBS analysis of the dried residue from

25 µL of concentrated, undiluted radiochemical process solution containing significant masses of

americium, curium, and rare earth and other fission products [48]. No ICP-based instrument

could measure this sample without multiple orders-of-magnitude dilution and resultant

propagation of analytical uncertainties. Since then, no comparable experiment has been reported

in the literature, but the results clearly indicated the need for an *a priori* comprehensive LIBS

spectral library to qualitatively predict spectral interferences and optimize the selection of

microvolume and mass content of the pipetted sample to facilitate subsequent data interpretation.

Because of the prolific atomic emission lines from the major rare earth fission products (in

addition to the even more prolific lines from any actinides present), **this work represents a**

significant step toward experimental planning of future LIBS analyses of real-world

nuclear samples.

The objective of this article is to:

- obtain the broadband LIBS emission spectra from single-element samples of six rare earth elements Eu, Gd, La, Nd, Pr, and Sm, and one transition metal Y, at concentrations of 1% and 50% by weight for each element in oxide form within a carbon matrix. This has allowed the authors to identify the specific peaks for each element and develop a calibration curve for each.

- develop multivariate calibration and cross-validations for each individual element (shown in table 3) and,

- obtain the broadband LIBS emission spectrum from an equal mixture of the rare earth elements, Eu, Gd, La, Nd, Pr, and Sm, and one transition metal Y to see if individual emission lines from these can be identified in this mixture.

2 Experimental

LIBS is a laser-based technique in which, for this study, a laser of 532 nm wavelength is focused onto the surface of a sample which vaporizes and ionizes a small volume of sample material to generate a plasma spark. All states of matter can be analyzed; e.g., solid, liquid, gaseous, and aerosol. LIBS vaporizes a small sample volume with sufficient energy to ionize all elemental components into optically excited states in the resultant sample plume. The vaporized species then undergo de-excitation and optical emission on a microsecond time scale, and time-dependent ultraviolet-visible spectroscopy fingerprints the elements associated with the spectral peaks. The plasma emits light that is collected by an optical fiber and delivered to a spectrometer. The spectrometer separates out the white light of the plasma into different

wavelengths, and coupling onto the face of an intensified charge coupled device (ICCD) detector converts the optical signal into an electronic signal. Powerful computer software is used to present a spectrum (intensity versus wavelength) of the sample under test. The process of excitation, light collection, separation into wavelengths, and optical signal conversion to electronic signal is completed within 100 milliseconds. LIBS is typically a surface analytical technique, with each laser pulse vaporizing microgram or submicrogram sample masses. However, the rapidity of sampling (typically 10 Hz laser repetition rate) and ability to scan a sample surface, ablate a hole into a solid sample with repeated laser pulses (for depth profiling) or focus the laser spark below the surface of a liquid sample permits more versatile analyses and provides sufficient statistics for bulk sampling. The detection limits are often in the parts per million (1 ppm to100 ppm) range for most elements in the periodic table (dependent on sample matrix). These limits of detection can be reduced when the sample is placed under reduced atmospheric pressure or in an inert gaseous environment.

2.1 Instrumentation

The main components of the experimental system are a pulsed Big Sky laser model CFR-Ultra which is a Q-switched Nd:YAG laser with frequency doubled output wavelength of 532 nm [28]. Laser energy of 45 mJ was used to obtain all the sample spectra. The experimental setup also has an X-Y-Z stage to provide capability of three-dimensional movements. A displacement laser (650 nm) is employed to control the vertical position of the sample upper surface, making sure that the laser beam which is exciting the sample surface remains focused and that the plasma is optimally located with respect to the collection optics. The light emitted by the plasma at the focal volume was collected by a set of collection optics and focused into a low O-H silica fiber. The optical fiber is used to deliver the light to an Echelle spectrometer

from Catalina Scientific model SE 200 spectrometer that resolves light into different

wavelengths by a high order dispersion module (190-800 nm range), followed by detection using

a 2-D 1024x1024 pixel intensified charge coupled detector (ICCD) made by Andor

Technologies. The advantage of using an ICCD is that the detection can be delayed with respect

to plasma formation. The data was collected by using a delay of 1 microsecond, a gate width of

10 microseconds, and the repetition rate at which the laser was operated was 10 Hz. The whole

process of sample excitation, plasma formation, light collection, and optical-to-digital conversion

of the signal takes at most a second to a few seconds depending on the number of shots that are

averaged to get a good signal–to-noise ratio. Table 1 summarizes the laser and

detector/spectrometer characteristics.

Table1. Characteristics of laser and detector/spectrometer.

Laser Characteristics					
Wavelength	Energy/pulse	Rep- rate			
532 nm	45mJ	10 Hz			
Detector/Spectrometer Characteristics			Pixel resolution (FWHM) nm		
Wavelength range nm	Practical spectral bandwidth		200-400	400-600	600-800
190-800	210-790 nm		0.06	0.06-0.08	0.09-0.12

2.2 Reagents

All the rare earth oxide powders (Eu_2O_3, Gd_2O_3, La_2O_3, Nd_2O_3, Pr_6O_{11}, Sm_2O_3, and the

transition metal oxide Y_2O_3), were obtained from Alpha Aesar, Ward Hill, Massachusetts (USA).

The purity of the oxide powders that were used in this research was 99.99%. The graphite
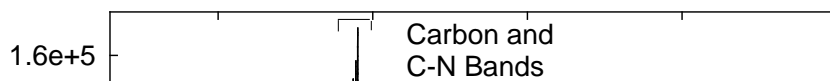
powder that was a natural, microcrystal grade, of 99.9995% purity was also obtained from Alpha

Aesar, Ward Hill, Massachusetts (USA). The polyvinyl acetate (PVA) was 99-100%

hydrolyzed, and was obtained from Acros Organics, New Jersey, USA.

2.3 Preparation of samples

The powders of the rare earth oxides Eu_2O_3, Gd_2O_3, La_2O_3, Nd_2O_3, Pr_6O_{11}, Sm_2O_3, and the

transition metal oxide Y_2O_3 were used in making the pellets. These powders were weighed along

with a balancing amount of graphite powder diluent. The total weight of the oxide material and

graphite mixture was 75 mg. These components were combined in a bottle and the mixture

vortexed and stirred. A quantity of 300 uL of 0.5% PVA solution was pipetted into a glass tube

and re-mixed a second time as in the previous step. A heating block was used to dry the mixed

powders containing PVA. The contents of the bottle were emptied into a 1/4" die and pressed at

1500 1b for at least one minute. The pellets were placed in a labelled plastic bag until

subsequent LIBS measurements.

3. Results and Discussions

LIBS spectra obtained using an Echelle spectrometer for 1% by weight of each of the rare

earth (Eu, Gd, La, Nd, Pr, and Sm) and Y (transition metal) oxides, mixed with a 99% balance of

graphite powder are shown in figure 1(a). The elemental concentrations range from 0.79% for Y

to 0.87% for Gd. The acquired range of the spectra is 200-800 nm (reduced to 250-700 nm

here), obtained under an argon purge atmosphere. The spectra are very complex with a dense

distribution of spectral features that are extremely difficult and tedious to identify individually.

Since the buildup of fission product elements from nuclear fission

1.6e+5 ─┤   Carbon and
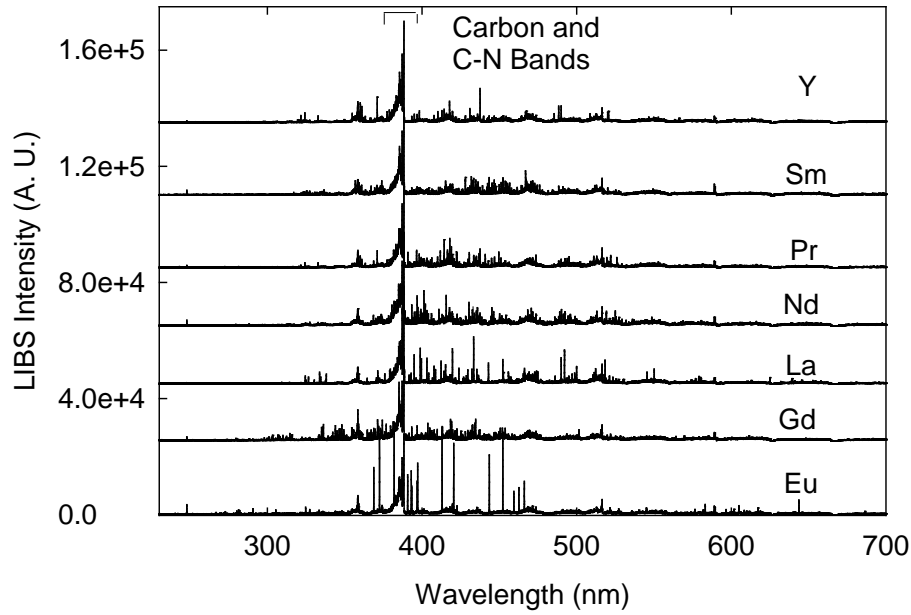   C-N Bands

Figure 1 (a). LIBS spectra for 1% concentration of Eu, Gd, La, Nd, Pr, Sm, and Y oxides individually in graphite matrix.

reactions can be as high as 18 % of the total fissions for Nd, figure 1(b) shows the spectra of 25% by weight of each element's oxide (with elemental concentrations ranging from19.7% for Y to 21.7% for Gd), in which the complexity and density of peaks increase rapidly over the 1% spectra shown in figure 1(a). By zooming into the spectral region of interest the individual spectral lines can be clearly observed as shown in figure 1(c). Due to the density of the number
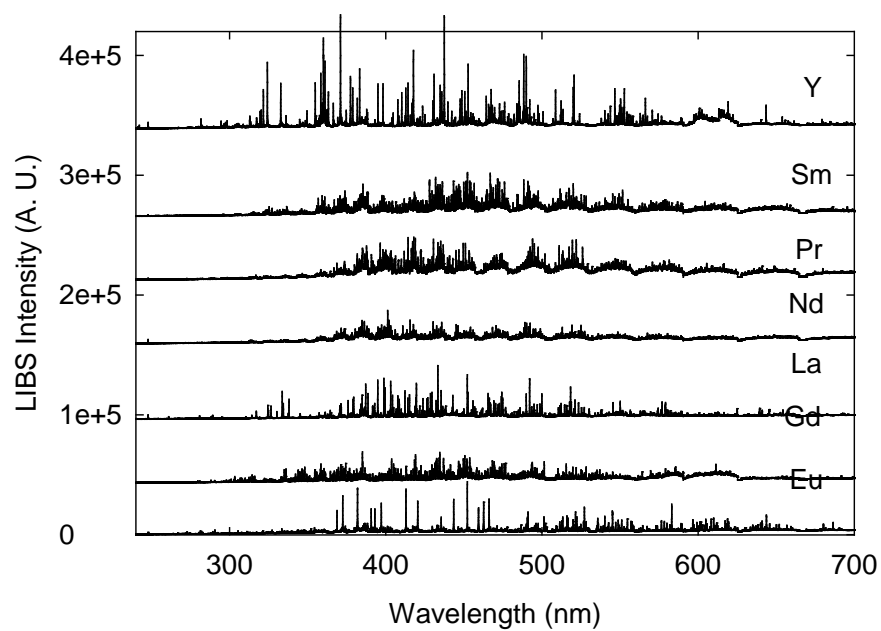
of spectral lines, some line interferences are observed.

Figure 1 (b). LIBS spectra for 25% concentration of Eu, Gd, La, Nd, Pr, Sm, and Y oxides individually in graphite matrix.
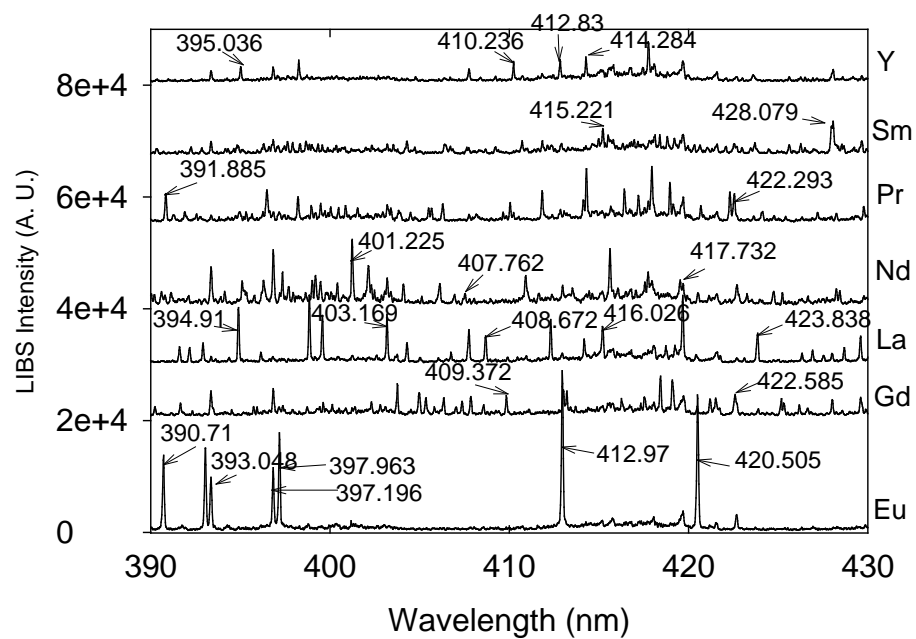

.

Figure 1 (c). LIBS spectra for 25% concentration of Eu, Gd, La, Nd, Pr, Sm, and Y oxides in the expanded wavelength window of 390-430 nm.

The main neutral and ionic lines of the rare earths have been identified in the expanded wavelength region (390-430 nm) in figure 1(c). This spectrum shows that multiple signature peaks for fingerprinting each rare earth element can be used in calibrating these individual elements.   When we correlate the peaks in the LIBS spectra to the NIST-Atomic spectra data base lines, the peaks that were identified for Y are 393.066, 395.036, 398.26, 407.735, 410.236, 412.83, 414.284, 417.754, and 419.928 nm. The peaks identified for Sm are 392.828, 411.019, 411.855, 415.221, 419.945, and 428.079 nm. The peaks that were identified for Pr are 391.885, 396.426, 398.051, 398.968, 399.583, 405.88, 410.073, 411.389, 414.311, 416.804, 417.225, 417.939, and 422.293 nm. For Nd, the peaks of interests were 392.71, 395.745, 397.33, 397.949, 399.01, 401.225, 402.478, 404.08, 406.109, 407.762, 410.946, 415.626, and 417.732 nm. A number of peaks identified for La are 392.922, 394.91, 398.852, 399.575, 403.169, 404.291, 407.735, 408.672, 412.323, 415.197, 416.026, 419.655, and 423.838 nm. The peaks that were identified for Gd are 396.929, 404.684, 405.364, 405.822, 407.87, 409.372, 418.425, 419.078, and 422.585 nm and lastly the peaks correlated to Eu are 390.71, 392.887,393.048, 397.196, 397.963, 412.97, 420.505 nm (figure 1(c)). All the peaks that are mentioned here have not been shown in figure 1(c) because of the scaling for the seven spectra it was difficult to label them individually. This shows that even in a small wavelength range, we have a cluster of 70 peaks that can be used to identify definitively the set of seven elements that have been studied for this article
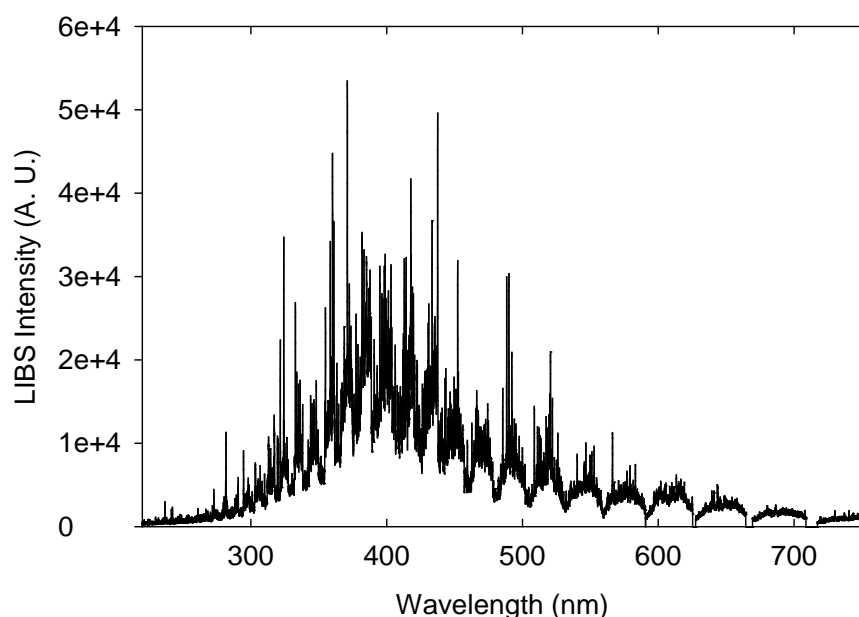
Figure 2(a). LIBS spectrum for a mixture of equal masses of Eu, Gd, La, Nd, Pr, Sm, and Y oxides.

Figure 2(a) shows the full broad-band spectrum of an equal mixture of Eu, Gd, La, Nd, Pr, Sm, and Y oxides. The concentration of each oxide is 14.3% (elemental concentrations range from 11.3% Y to 12.4% Gd). After acquiring the data for this mixture, it was noticed that the complexity and richness of the spectral features increased greatly, as expected. To see if we can differentiate all seven rare earths within this complex mixture, the spectrum is expanded within the wavelength region of 220-300 nm in figure 2(b). After expanding the broadband spectrum to focus on a smaller window, it was observed that individual peaks of Eu, Pr, and Y could be resolved. Further investigation of the wavelength region between 350-400 nm (figure 2(c)) demonstrates that all seven elements can be identified in this region. Similarly, all seven elements can be identified in the wavelength region between 350-450 nm (figure 2 (c and d)).
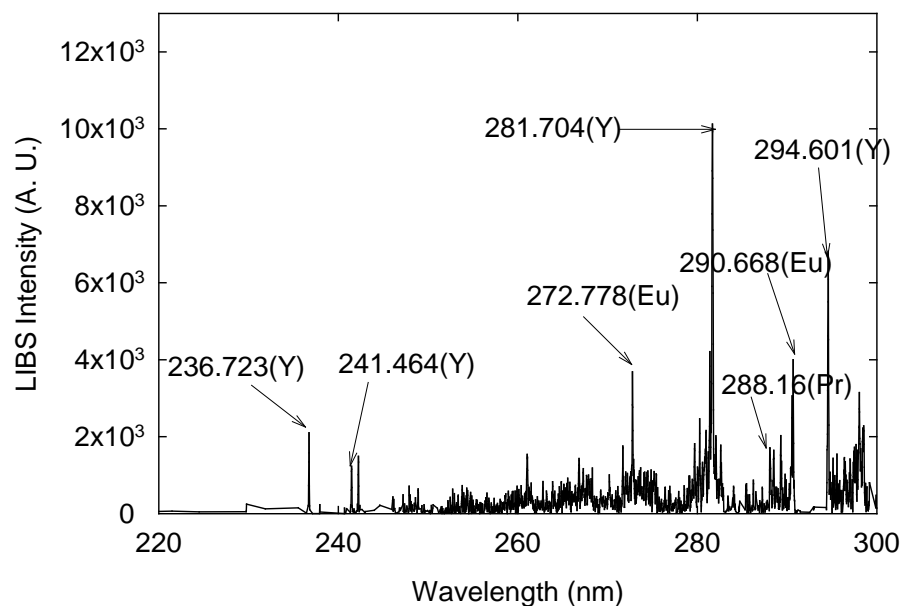
Figure 2(b). LIBS spectrum for a mixture of equal masses of Eu, Gd, La, Nd, Pr, Sm, and Y

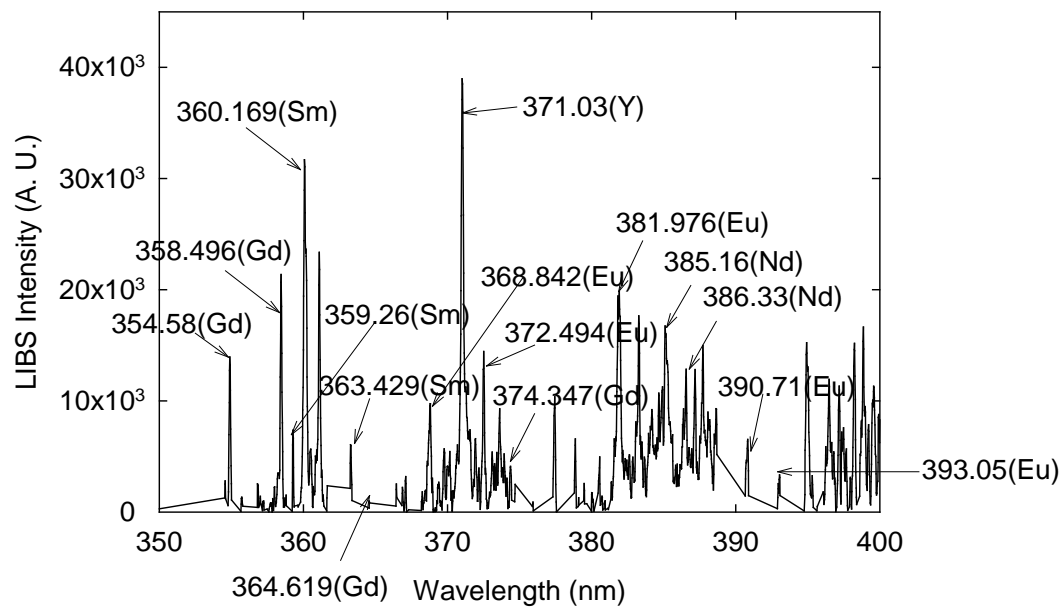oxides expanded into a wavelength window from 220-300 nm.

Figure 2(c). LIBS spectrum for a mixture of equal masses of Eu, Gd, La, Nd, Pr, Sm, and Y

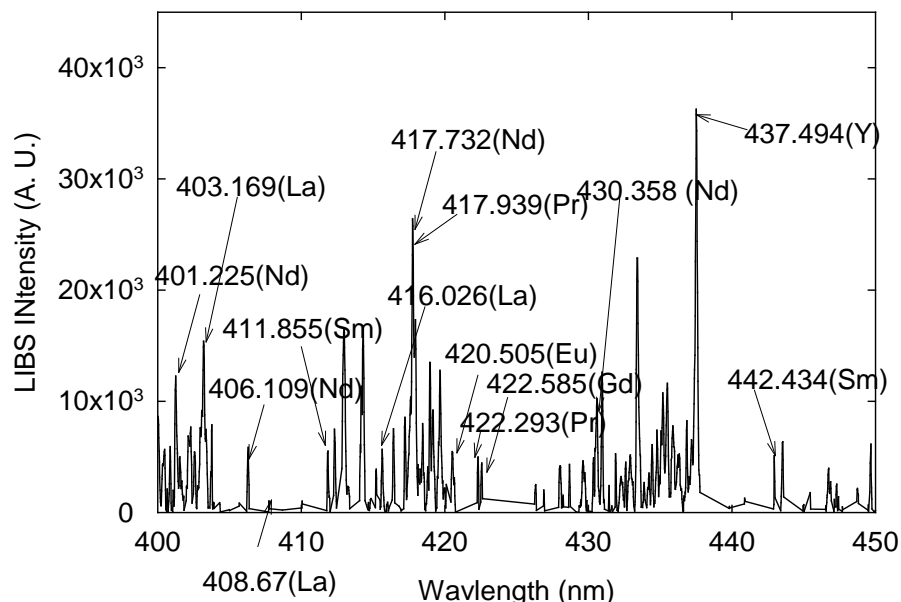oxides expanded into a wavelength window from 350-400 nm

Figure 2(d). LIBS spectrum for a mixture of equal masses of Eu, Gd, La, Nd, Pr, Sm, and Y

oxides expanded into a wavelength window from 400-450 nm.

Armed with this information, it was concluded that univariate analysis is impractical

when analyzing complex mixtures such as those reported in this article. Picking the best spectral

features from each element is a tedious and time-consuming task, especially if developing

calibration curves for each individual element and then extrapolating that information to the

entire mixture of rare earths. In the case of each of the seven elements, six spectra of

concentrations each from 1% -50% were obtained for each rare earth oxides mixed with the

balance of graphite powder. Hence partial least square (PLS) was used for the element

concentration determination. PLS is a multivariate analysis (MVA) technique that provides a

model for the relationship between a set of predictor variables X (*n* objects, *m* variables) and a

set of response variables Y (*n* objects, *p* responses) [49]. In this case, *m* variables are the LIBS

wavelengths and *p* responses are properties such as the concentrations for the six rare earths and

one transition metal. The *p* response must be independently measured for each sample. If the

spectral data contain information about the properties of interest, a reliable calibration model can

be constructed. Multivariate analysis of the data is performed using the Unscrambler

(version 9.7) software, CAMO, Corvallis, OR [50]. Three important results in using this

approach are (1) the r^2 coefficient of determination for the calibration and validation, (2) the

loading parameters for each element which should be examined in detail to verify if the features

that were selected by the PLS model are real peaks attributed to the specific elements, and (3) the

number of principal components (PCs) that the model uses for prediction of those elements. In

general, the lower the number of PCs, the better is the development/construction of the model. If

the numbers of PCs are greater than 10 to 15, then there is the danger of integrating on the

features in the noise of the spectra and not on the real peaks. A PLS model is used to determine

the correlation between measured and predicted rare earth content from the laser-induced

breakdown spectra. Figure 3(a) depicts the predicted versus measured Eu, Gd, La, and Nd

scatter plots for the calibration (all samples) and full cross-validation sample sets. Excellent

coefficients of determination (r^2) were found for the calibration for each element with 0.97, and

0.95, and 0.97, and 0.98, respectively. Full cross-validation results were slightly lower with

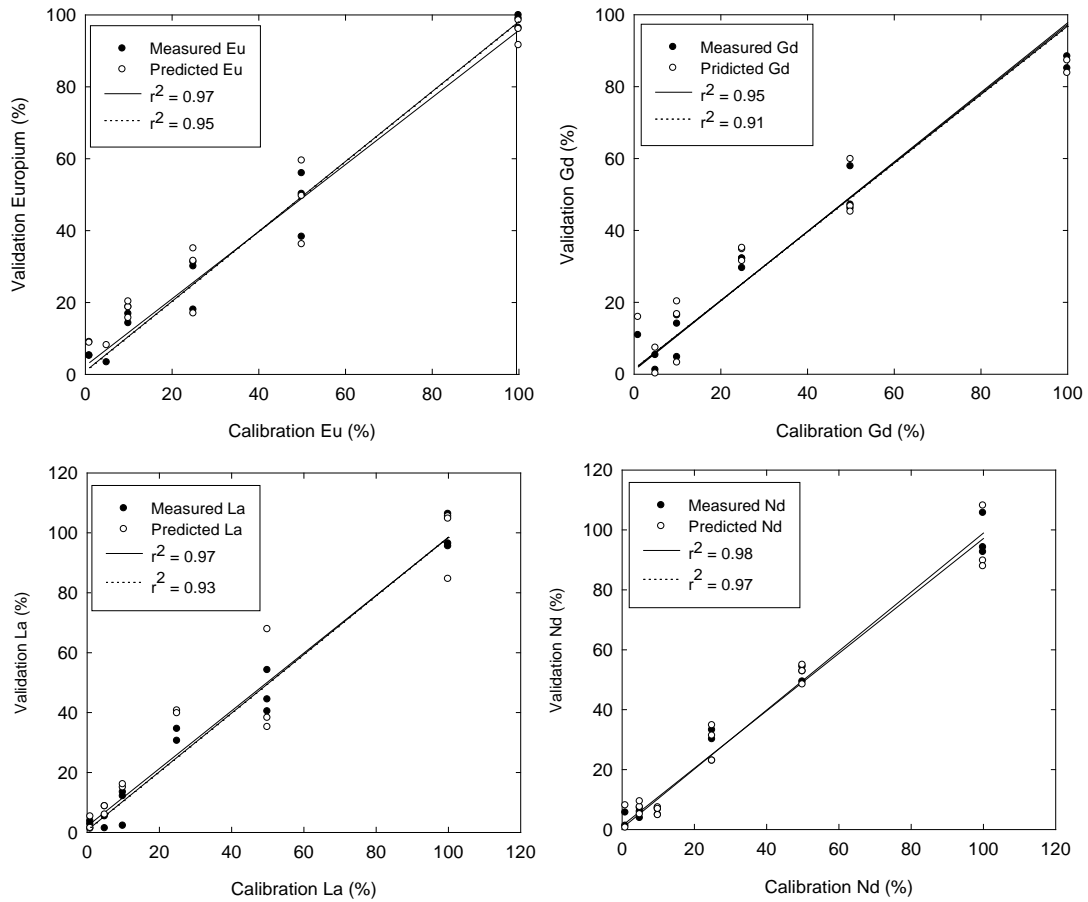0.95, 0.91, 0.93, and 0.97 respectively.

Figure 3(a). r^2 – coefficient of determination for calibration and full cross-validation sample sets for Eu, Gd, La, and Nd.

Figure 3(b) depicts the predicted versus measured multivariate regression curves for Pr, Sm, and Y scatter plots for the calibration and full cross-validation sample sets. Excellent coefficients of determination (r^2) were found for the calibration sample set for each element with 0.99, 0.97, and 0.99, respectively. Full cross-validation results were slightly weaker (especially

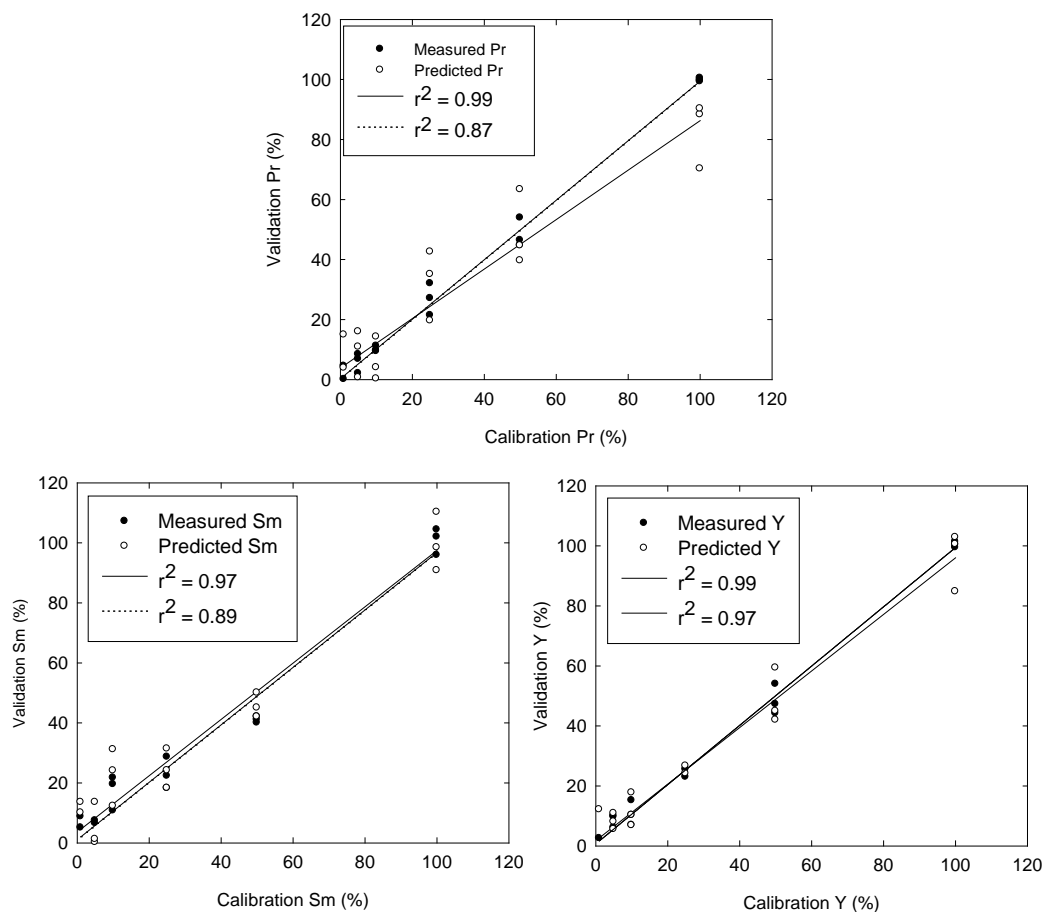for Pr and Sm), with 0.87, 0.89, and 0.97, respectively.

Figure 3(b). r^2 – coefficient of determination for calibration and full cross-validation for Pr, Sm, and Y.

PLS regression models help identify the spectral features present in these rare earth oxide mixtures that contribute to the PLS regression models, in which case acceptable regression coefficients are obtained for both calibration and validation models. No pre-treatment of data was undertaken. Out of the total six spectra that were acquired for each element at each concentration, three were used for calibration and the remaining three were used for validation. PLS1 was performed along with calibration and full cross-validation. PCA was done to find the

outliers for each element and those were eliminated from the calibration set. This is shown in

Table 2. below.

Table 2. Regression coefficients, offsets, and root mean square error (RMSE) for both calibration and validation sets for Eu, Gd, La, Nd, Pr, Sm, and Y.

Element	Slope	Offset	RMSE	R-Square
Eu (Calibration)	0.973	0.87	5.73	0.973
Eu (Validation)	0.933	2.37	8.09	0.951
Gd (Calibration)	0.954	1.47	7.43	0.954
Gd (Validation)	0.967	1.06	10.4	0.913
La (Calibration)	0.988	0.68	5.17	0.979
La (Validation)	0.964	2.05	10.06	0.929
Nd (Calibration)	0.985	0.48	4.27	0.985
Nd (Validation)	0.958	1.27	6.04	0.973
Pr (Calibration)	0.992	0.26	3.14	0.992
Pr (Validation)	0.824	3.88	12.16	0.875
Sm (Calibration)	0.969	1.02	6.30	0.968
Sm (Validation)	0.920	1.97	12.25	0.896
Y (Calibration)	0.993	0.22	2.88	0.993
Y (Validation)	0.944	1.62	6.75	0.969

Figure 4 shows the loading parameters for all seven rare earth and transition elements that have

been identified as the contributing features in distinguishing the rare earth and transition
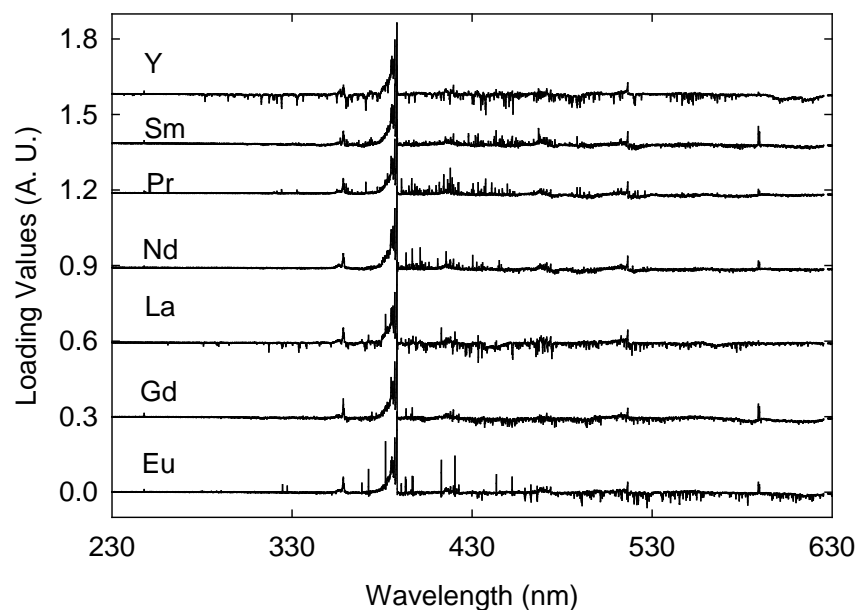
elements between each other.

Figure 4. The loading parameters for Eu, Gd, La, Nd, Pr, Sm and Y.

. Table 3 below summarizes the loading parameters for the different elements that the calibration-validation methodology has identified in the wavelength range 390-430 nm.

Table 3.

Element	Observed Wavelength (nm)	Element	Observed Wavelength (nm)	Element	Observed Wavelength (nm)
Eu(II)	390.71	La(I)	416.026	Pr(II)	422.293
Eu(II)	392.887	La(II)	419.655	Sm(II)	392.828
Eu(II)	393.048	La(II)	423.838	Sm(II)	411.019
Eu(II)	397.196	Nd(II)	392.710	Sm(II)	411.855
Eu(II)	397.963	Nd(II)	395.745	Sm(II)	415.221
Eu(II)	412.97	Nd(II)	397.330	Sm(II)	419.945
Eu(I)	413.707	Nd(II)	397.949	Sm(II)	428.079
Eu(II)	420.505	Nd(II)	399.010	Y(II)	393.066
Gd((II)	396.929	Nd(II)	401.225	Y(II)	395.036
Gd(II)	404.684	Nd(II)	402.478	Y(II)	398.260
Gd(I)	405.364	Nd(II)	404.080	Y(I)	407.735
Gd(I)	405.822	Nd(II)	407.762	Y(I)	410.236

GdI)	407.870	Nd(II)	410.946	Y(I)	412.830
Gd(I)	409.372	Nd(II)	415.626	Y(I)	414.284
Gd(II)	418.425	Nd(II)	417.732	Y(II)	417.754
Gd(I)	419.078	Pr(II)	391.885	Y(II)	419.928
Gd(I)	422.585	Pr(II)	396.426		
La(II)	392.922	Pr(III)	398.051		
La(II)	394.91	Pr(II)	398.968		
La(II)	398.852	Pr(II)	399.585		
La(II)	399.575	Pr(II)	405.880		
La(II)	403.169	Pr(II)	410.072		
La(II)	404.291	Pr(II)	411.389		
La(II)	407.735	Pr(II)	414.311		
La(II)	408.672	Pr(II)	416.804		
La((II)	412.323	Pr(II)	417.225		
La(II)	415.197	Pr(II)	417.939		

The first observation is that the PLS1 model selected very few features in the spectra as compared to the original dense, complex features. The prominent loading parameters for these elements are shown in figure 4. The spectral features listed in table 3 are the loading parameters picked out by the program to distinguish the seven elements from each other. The next parameter to be calculated is the total residual variance plot for the seven elements. The total residual variance plot should be a decreasing function of the number of components. Figure 5(a) presents the total residual variance plots and is used to assess where the model structure stops and the noise starts for all the correlations. For example, the first graph is the distribution of Eu variation between the different PCs. The second graph in figure 5(a) shows the distribution of the variation of Gd data between the different PCs, and the third graph is the distribution of the variation of La data between the different PCs. All the graphs show that most of the variations in the features that contribute to the residual validation model lie within the PC1 components and less variation is found between PC1 and PC2. Even less variation of the features that contribute to the residual validation model is found between PC2 and PC3, and then the variation decreases

as expected between PC3 and PC4. This continues until no variation is observed for higher order

PCs. The basic PC selection assumes that inclusion of "small" variations do not correspond to

significant data structure(s), but rather to noise. That is why it is important to have fewer PCs to
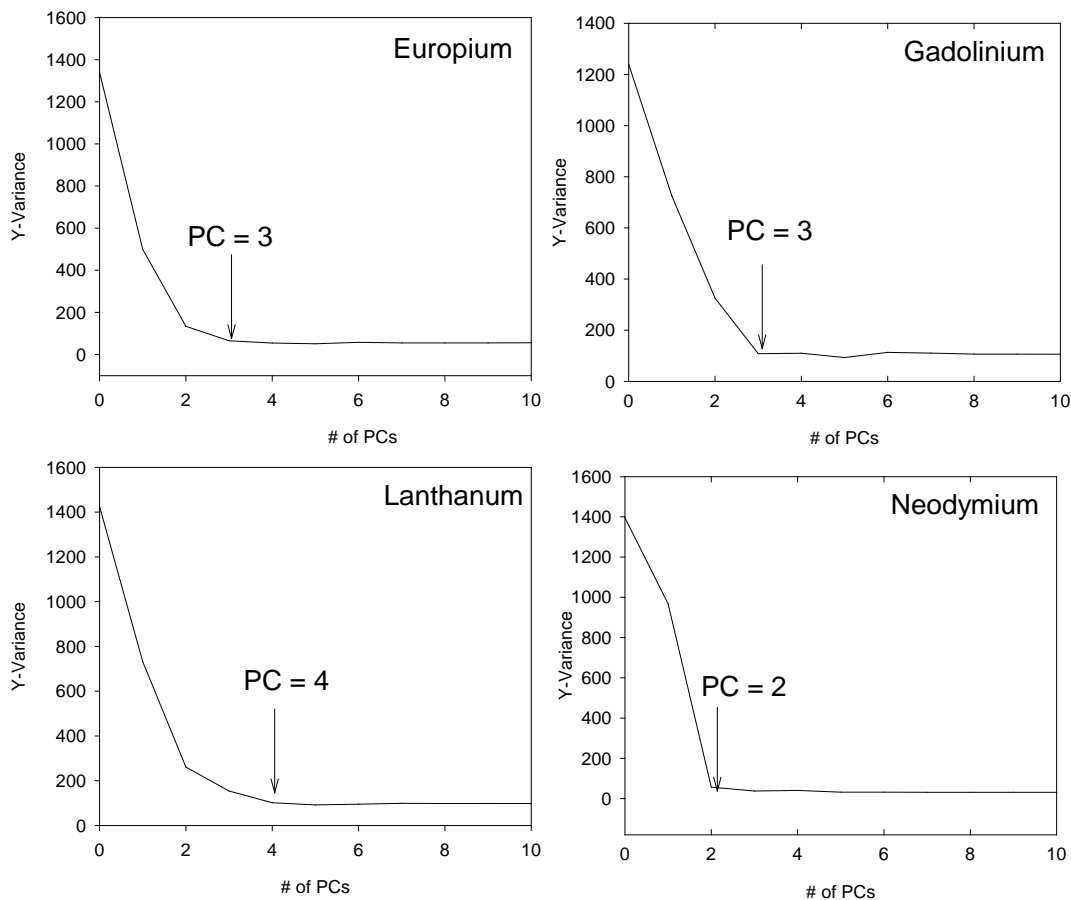
develop a robust model.

Fig. 5(a). Distribution of Eu, Gd, La, and Nd variation between the different principal

components (PCs).

Similarly in figure 5(b), the first graph depicts the PC variation reduced to background for PC=6

and in the other graphs the PC number is 4 for samarium and finally for yttrium the PC = 4 at
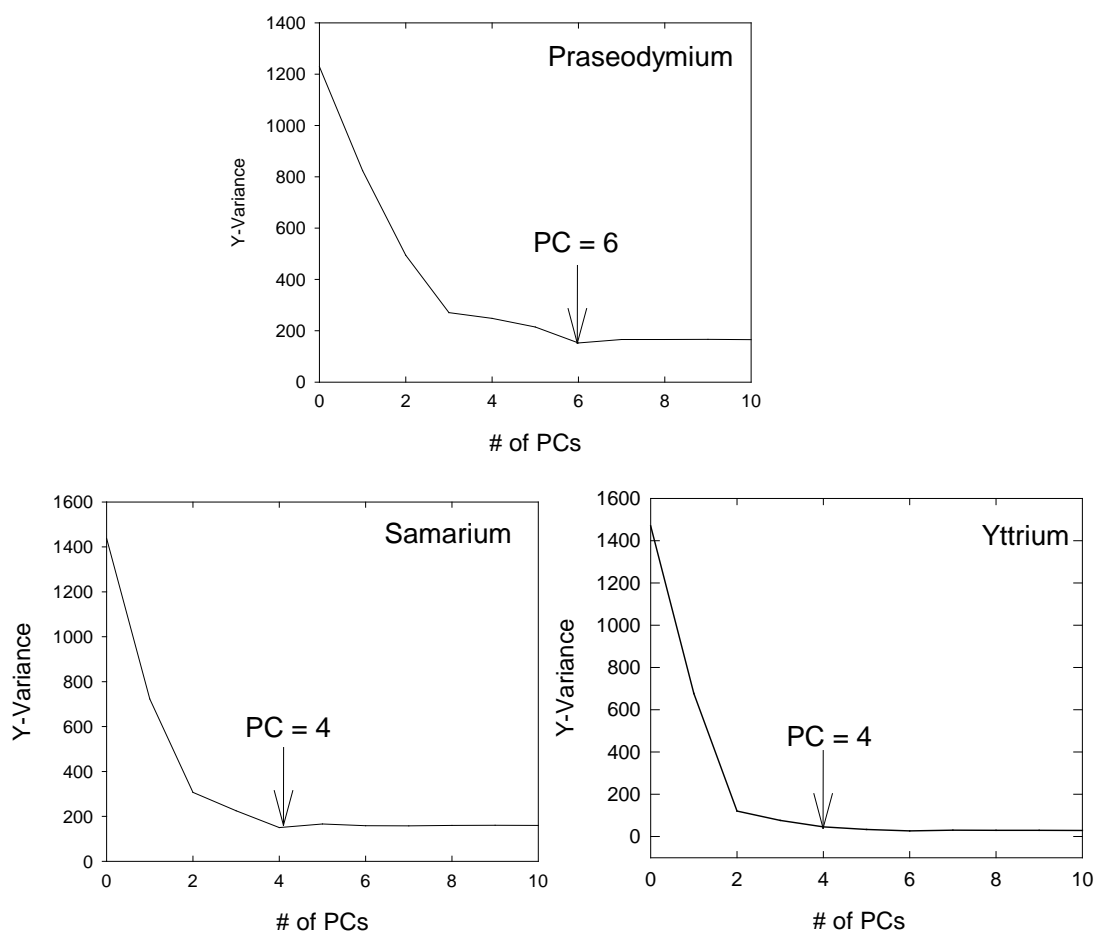
which the variation is completely stabilized.

Fig. 5(b). Distribution of Pr, Sm, and Y variation between the different principal components (PCs).

4. Conclusions

LIBS was used to obtain the complex emission spectra from single-element samples of six rare earth elements Eu, Gd, La, Nd, Pr, and Sm, and one transition metal Y, at concentrations of 1% and 50% by weight for each element in oxide form. Multivariate calibration and cross-validation correlations were developed for each individual element. The calibration r^2 for each

element were very good, with values ranging from 0.95 to 0.99. The cross-validation r^2 for each element were slightly lower, with values ranging from 0.87 to 0.97 which is to be expected. A multivariate approach was developed for each element of interest and was able to determine those features that were the primary contributors to the mixed spectra from each specific element. The variation of all the elements between different principal components was found to be between 3 and 6 components, hence confirming that the statistical methodology is very robust and stable. Finally, the loading parameters were confirmed as picked by the PLS multivariate analysis model.

5. Acknowledgements

6. References

[1]   S. D. Herrmann, S. X. Li, M. F. Simpson, and S. Phongikaroon, Electrolytic Reduction of Spent Nuclear Oxide Fuel as Part of an Integral Process to Separate and Recover Actinides from Fission Products, Separation Sci. and Technol., 41, (2006) 1965-1983.

[2]   Jong-Il Yun, R. Klenze, and Jae-Il Kim, Laser-Induced Breakdown Spectroscopy for the On-line Multielement Analysis of Highly Radioactive Glass melt. Part I: Characterization and Evaluation of the Method, Appl. Spectrosc., 56(4) (2002) 437-448.

[3]   Jong-Il Yun, R. Klenze, and Jae-Il Kim, Laser-Induced Breakdown Spectroscopy for the On-line Multielement Analysis of Highly Radioactive Glass melt. Part II: Analyses of Molten Glass Samples, Appl. Spectrosc., 56(7) (2002) 852-858.

[4]   C. A. Smith, M. A. Martinez, D. K. Veirs, and D. A. Cremers, Pu-239/Pu-240 isotope ratios determined using high resolution emission spectroscopy in a laser-induced plasma", Spectrochimica Acta B57 (2002) 929-937.

[5]   D. A. Cremers, A. Beddingfield, R. Smithwick, R. Chinni, C. R. Jones, B. Beardsley, and L. Karch,Monitoring Uranium, Hydrogen, and Lithium and Their Isotopes Using a Compact Laser-Induced Breakdown Spectroscopy (LIBS) Probe High-Resolution Spectrometer, Appl. Spectrosc., 66(3) (2012) 250-261.

[6]   J. E. Barefield II, E. J. Judge, J. M. Berg, S. P. Willson, L. A. Le, and L. N. Lopez, Analysis and Spectral Assignments of Mixed Actinide Oxide Samples Using laser-Induced Breakdown Spectroscopy (LIBS), Appl. Spectrosc., 67(4) (2013) 433-440.

[7]   E. J. Judge, J. E. Barefield II, J. M. Berg, S. M. Clegg, G. J. Havrilla, V. M. Montoya, L. A. Le, and L. N. Lopez, "Laser-induced breakdown spectroscopy measurements of uranium and thorium powders and uranium ore," Spectrochimica Acta B, 83-84 (2013) 28-36.

[8]   T. Bundschuh, Jong-Il Yun, and R. Knopp, "Determination of size, concentration and elemental composition of colloids with laser-induced breakdown detection/spectroscopy (LIBD/S)," Fresnius J Anal. Chem., 371 (2001) 1063-1069.

[9]   D. Alamelu, A. Sarkar, S. K. Aggarwal, Laser-induced breakdown spectroscopy for simultaneous determination of Sm, Eu, and Gd in aqueous solutions, Talanta 77 (2008) 256-261.

[10]   Jong-Il Yun, T. Bundschuh, V. Neck, and Jae-Il Kim, Selective Determination of Europium (III) Oxide and HydroxideColloids in Aqueous Solution by Laser-Induced Breakdown Spectroscopy, Appl. Spectrosc., 55(3) (2001) 273-278.

[11]   E. C. Jung, D. H. Lee, J.-I Yun, J. G. Kim, J. W. Yeon, and K. Song, Quantitative determination of uranium and europium in glass matrix by laser-induced breakdown spectroscopy, Spectrochimica Acta B 66(9-10) (2011) 761-764.

[12]   H. Hotokezaka, S. Tanaka, A. Suzuki, and S. Nagasaki, Speciation analysis on europium (III) using laser-induced breakdown spectroscopy, Radiochimica Acta 88(9-10) (2000) 645-648.

[13]   D. Menut, P. Mauchien, Y.S. Gif , M. Descostes, P. Meier, J. Radwan, and C. Poinssot, Eu migration in Callovo-Oxfodian argillite: on the use of micro laser-induced breakdown

spectroscopy (micro LIBS) as a microanalysis tool, Int. conf. on chemistry and migration behavior of actinides and fission products in the geosphere; Avignon (France) vol. 38(27), 1-(Sept. 2005).

[14]   G. Zikratov, R. Vasudev, F. Y. Yueh, J. P. Singh, and J. C. Marra, Laser induced breakdown spectroscopy of hafnium doped vitrified glass, Glass Technol., 40(3) (1999) 84-88.

[15]   K. Song, D. Kim, H. K. Cha, Y. Kim, E. C. Jung, I. Choi, H. S. Yoo, and S. Oh, Characterization of laser-induced plasma in a vacuum using laser ablation mass spectrometry, and laser-induced breakdown spectrometry, Microchem. J., 76 (1-2) (2004) 95-103.

[16]   M. Oba, Y. Maruyama, K. Akaoka, M. Miyabe, I. Wakaida, Double-pulse LIBS of gadolinium oxide ablated by femto- and nano-second laser pulses, Appl. Phys. A 101 (2010) 545-549.

[17]   V. K. Unnikrishnan, R. Nayak, P. Devangad, M. M. Tamboli, C. Santhosh, G. A. Kumar, and D. K. Sardar, Calibration based laser-induced breakdown spectroscopy (LIBS) for quantitative analysis of doped rare earth elements in phosphors, Mat. lett, 107 (2013) 322-324.

[18]   S. H. Kim, J. S. Ju, Y. H. Lee, J. H. Jeong, and H. S. Sin, Semi-quantitative analysis of the Neodymium binary alloys using Laser induced breakdown spectroscopy, Trans. Korean Nucl. Soc., Autumn meeting PueongChang, Korea Oct 30-31 (2008).

[19]   S. J. Rehse and C. A. Ryder, Laser-induced breakdown spectroscopy for branching ratio and atomic lifetime measurements in singly-ionized neodymium and gallium, Spectrochimica Acta B., 64(10) (2009) 974-980.

[20]   A. F. M. Y. Haider, M. A. Rony, R. S. Lubna, and K. M. Abedin, Detection of multiple elements in coal samples from Bangladesh by laser-induced breakdown spectroscopy, Optics & Laser Technol., 43(8) (2011) 1405-1410.

[21]   S. H. Kim, J. S. Hong, J. S. Ju, and H. S. Sin, A quantitative analysis for Lanthanum series element using Laser induced breakdown spectroscopy, Trans. Korean Nucl. Soc., Spring meeting, Gyeongju, Korea May 29-30 (2008).

[22]   A. Ciucci, V. Palleschi, S. Rastelli, R. Barbini, F. Colao, R. Fontini, A. Palucci, S. Ribezzo, and H. J. L. van der Steen, Trace pollutants anlaysis in soil by a time-resolved laser-induced breakdown spectroscopy technique, Appl. Phys. B, 63(2) (1996) 185-190.

[23]   S. H. Kim, J. S. Ju, J. -H. Jeong, H. -S. Sin, and H. –D. Kim, Semi- quantitative analysis for Samarium alloys sample using Laser induced breakdown spectroscopy, Trans. Korean Nucl. Soc., Spring meeting, Jeju, Korea May 22 (2009).

[24]   J. Pigosova, A. Kilianova, P. Vojtek, M. Kopcok, and A. Cigan, Preparation of bismuth-doped yttrium iron garnets and their characterization. Proc. of SPIE 6609, M1-M7 2007.

[25]   S. G. Buckley, H. A. Johnson, K. R. Hencken, D. W. Hahn. Implementation of laser-induced breakdown spectroscopy as a continuous emissions monitor for toxic metals: Waste Management, 20(5-6) (2002) 455-462.

[26]   H. Zhang, F. –Y. Yueh, and J. P. Singh, laser-induced breakdown spectrometry as a
          multimetal continuous-emission monitor, Appl. Opt., 38(9) (1999)1459-1466.

[27]   K. M. Abedin, A. F. M. Y. Haider, M. A. Rony, and Z. H. Khan, Identification of
          multiple rare earths and associated elements in raw monazite sands by laser-induced
          breakdown spectroscopy, Optics & Laser Technol., 43(1) (2011) 45-49.

[28]   Madhavi Z. Martin, Steve Allman, Deanne J. Brice, Rodger C. Martin, Nicolas O. Andre,
          Exploring laser-induced breakdown spectroscopy for nuclear materials analysis and in-
          situ applications, Spectrochimica Acta Part B. vol 74-75 (2012) 177-183.

[29]   M. Benedict, T. H. Pigford, and H. W. Levi, Nuclear Chemical Engineering, 2nd ed.,

[30]   P.W.J.M. Boumans, Basic concepts and characteristics of ICP-AES, in: P.W.J.M.
          Boumans (Ed.), Inductively Coupled Plasma Emission Spectroscopy, Part 1,
          Methodology, Instrumentation, and Performance, Wiley, New York, 1987, p. 100, Chap.
          4.

[31]   P.W.J.M. Boumans, J.A. Tielrooy, F.J.M.J. Maessen, Mutual spectral interferences of
          rare earth elements in inductively coupled plasma atomic emission spectrometry-I.
          Rational line selection and correction procedure, Spectrochim. Acta Part B 43 (1988)
          173-199.

[32]   P.W.J.M. Boumans, J.J.A.M. Vrakking, A.H.M. Heijms, Mutual spectral interferences of
          rare earth elements in inductively coupled plasma atomic emission spectrometry-II
          Approach to the compilation and use of pseudo physically resolved spectral data,
          Spectrochim. Acta Part B 43 (1988) 1365-1488.

[33]   P.W.J.M.Boumans,He Zhi Zhuang, J.J.A.M.Vrakking, J.A.Tielrooy, F.J.M.J. Maessen, Mutual spectral interferences of rare earth elements in inductively coupled plasma atomic emission spectrometry-III. Pseudo physically resolved spectral data: complete results and evaluation, Spectrochim. Acta Part B 44 (1989) 31-93.

[34].   B. Huang, X. Wang, P. Yang, H. Ying, S. Gu, Z. Zhang, Z. Zhuang, Z. Sun,B. Li, An atlas of High Resolution Spectra of Rare Earth Elements for ICP-AES, Royal Society of Chemistry, 2000.

[35]   N. Daskalova, S. Velichkov, N. Krasnobaeva, P. Slavova, Spectral interferences in the determination of traces of scandium, yttrium and rare earth elements in "pure" rare earth matrices by inductively coupled plasma atomic emission spectrometry. Part I. Cerium, neodymium and lanthanum matrices, Spectrochim. Acta Part B 47 (1992) E1595-E1620.

[36]   S. Velichkov, N. Daskalova, P. Slavova, Spectral interferences in the determination of traces of scandium, yttrium and rare earth elements in "pure" rare earth matrices by inductively coupled plasma atomic emission spectrometry. Part II. Praseodymium and samarium, Spectrochim. Acta Part B 48 (1993) E1743-E1789.

[37]   N. Daskalova, S. Velichkov, P. Slavova, Spectral interferences in the determination of traces of scandium, yttrium and rare earth elements in "pure" rare earth matrices by inductively coupled plasma atomic emission spectrometry. Part III. Europium, Spectrochim. Acta Part B 51 (1996) 733-768.

[38]   S. Velichkov, E. Kostadinova, N. Daskalova, Spectral interferences in the determination of traces of scandium, yttrium and rare earth elements in "pure" rare earth matrices by

inductively coupled plasma atomic emission spectrometry, Part IV. Lutetium and yttrium. Spectrochim. Acta Part B 53 (1998) 1863-1888.

[39] E. Kostadinova, L. Aleksieva, S. Velichkov, N. Daskalova, Spectral interferences in the determination of traces of scandium, yttrium and rare earth elements in "pure" rare earth matrices by inductively coupled plasma atomic emission spectrometry, Part V. Gadolinium and Erbium, Spectrochim. Acta Part B 55 (2000) 689-729.

[40] L. Aleksieva, N. Daskalova, S. Velichkov, Spectral interferences in the determination of traces of scandium, yttrium and rare earth elements in "pure" rare earth matrices by inductively coupled plasma atomic emission spectrometry. Part VI. Ytterbium, Spectrochim. Acta Part B 57 (2002) 1341-1350.

[41]. I. Kolibarska, S. Velichkov, N. Daskalova, Spectral interferences in the determination of traces of scandium, yttrium and rare earth elements in "pure" rare earth matrices by inductively coupled plasma atomic emission spectrometry. Part VII — Terbium, Dysprosium, Holmium and Thulium, Spectrochimica Acta Part B 63 (2008) 603-606 McGraw-Hill, N.Y., 1981.

[42] B. C. Windom and D. W. Hahn, Laser ablation- laser induced breakdown spectroscopy (LA-LIBS): A means for overcoming matrix effects leading to improved analyte response, Journal of Analytical Atomic Spectrometry 24 (2009) 1665-1675.

[43] D. W. Hahn and N. Omenetto, Laser-induced breakdown spectroscopy (LIBS), Part I: Review of basic diagnostics and plasmaparticle interactions: Still-challenging issues within the analytical plasma community, Appl. Spectrosc. 64, 335A (2010) (review article)

[44]   D. W. Hahn and N. Omenetto, Laser-induced breakdown spectroscopy (LIBS), part II: review of instrumental and methodological approaches to material analysis and applications to different fields," Applied Spectroscopy, vol. 66, no. 4, pp. 347-419, 2012 (review article).

[45]   Bassiotis, A. Diamantopoulou, A. Giannoudakos, F. Roubani-Kalantzopoulou, and M. Kompitsas, "Effects of experimental parameters in quantitative analysis of steel alloy by laser-induced breakdown spectroscopy," Spectrochimica Acta Part B, vol. 56, no. 6, pp. (2001) 671-683.

[46]   F. Anabitarte, A. Cobo, and J.M. Lopez-Higuera, Laser-Induced Breakdown Spectroscopy: Fundamentals, Applications, and Challenges, International Scholarly Research Network ISRN Spectroscopy Volume 2012, Article ID 285240, 12 pages doi:10.5402/2012/285240 (review article).

[47]   R. A. Multari, L. E. Foster, D. A. Cremers, and M. J. Ferris, "Effect of sampling geometry on elemental emissions in laser-induced reakdown spectroscopy," Applied Spectroscopy, vol. 50, no. 12 (1996) pp. 1483-1499.

[48]   L. K. Felker, M. Z. Martin, J. Miller, and R. C. Martin, unpublished data, Oak Ridge National Laboratory, 2003.

[49]   http://www.camo.com/introducer/see-inside-multivariate-data-analysis.pdf

[50]   H. Martens and T. Naes, Multivariate Calibration, first ed. John Wiley and Sons, New York, 1989.

List of Figure Captions

Fig. 1(a). LIBS spectra for 1% concentration of Eu, Gd, La, Nd, Pr, Sm, and Y oxides

individually in a graphite matrix.

Fig. 1(b). LIBS spectra for 25% concentration of Eu, Gd, La, Nd, Pr, Sm, and Y oxides

individually in a graphite matrix.

Fig. 1 (c). LIBS spectra for 25 % concentrations of Eu-Gd, La, Nd, Pr, Sm, and Y oxides in the

expanded wavelength window of 390-430 nm.

Fig. 2 (a). LIBS spectrum for a mixture of equal masses of Eu, Gd, La, Nd, Pr, Sm, and Y

oxides.

Fig. 2 (b). LIBS spectrum for a mixture of equal masses of Eu, Gd, La, Nd, Pr, Sm, and Y oxides

expanded into wavelength window from 220-300 nm.

Fig. 2 (c). LIBS spectrum for a mixture of equal masses of Eu, Gd, La, Nd, Pr, Sm, and Y oxides

expanded into a wavelength window from 350-400 nm.

Fig. 2 (d). LIBS spectrum for a mixture of equal masses of Eu, Gd, La, Nd, Pr, Sm, and Y oxides

expanded into a wavelength window from 400-450 nm.

Fig. 3 (a). r^2 – coefficient of determination for calibration and full cross-validation sample sets

for Eu, Gd, La, and Nd.

Fig. 3 (b). r^2 – coefficient of determination for calibration and full cross-validation sample sets

for Pr, Sm, and Y.

Fig. 4. The loading parameters for Eu, Gd, La, Nd, Pr, Sm, and Y.

Fig. 5 (a). Distribution of Eu, Gd, La, and Nd variation between the different principal components (PCs).

Fig. 5 (b). Distribution of Pr, Sm, and Y variation between the different principal components (PCs).

List of Tables.

Table 1. Characteristics of laser and detector/spectrometer.

Table 2. Regression coefficients, offsets and root mean square error (RMSE) for both calibration and validation sets for Eu, Gd, La, Nd, Pr, Sm, and Y.

Table 3. Loading parameters for the different elements identified by the calibration-validation methodology in the wavelength range 390-430 nm.